UNIVERSITÄT AUGSBURG
Universitätsbibliothek

OPEN ACCESS
OPUS AUGSBURG

A study on the density shoulder formation in the SOL of H-mode plasmas

D. Carralero, J. Madsen, S. A. Artene, M. Bernert, Gregor Birkenmeier, T. Eich, G. Fuchert, F. Laggner, V. Naulin, P. Manz, N. Vianello, E. Wolfrum

Angaben zur Veröffentlichung / Publication details:

Carralero, D., J. Madsen, S. A. Artene, M. Bernert, Gregor Birkenmeier, T. Eich, G. Fuchert, et al. 2017. "A study on the density shoulder formation in the SOL of H-mode plasmas." *Nuclear Materials and Energy* 12: 1189–93. https://doi.org/10.1016/j.nme.2016.11.016.

Nutzungsbedingungen / Terms of use:

CC BY-NC-ND 4.0

Dieses Dokument wird unter folgenden Bedingungen zur Verfügung gestellt: / This document is made available under these conditions:
CC-BY-NC-ND 4.0: Creative Commons: Namensnennung - Nicht kommerziell - Keine Bearbeitung
Weitere Informationen finden Sie unter: / For more information see:
https://creativecommons.org/licenses/by-nc-nd/4.0/deed.de

Nuclear Materials and Energy 12 (2017) 1189–1193

Contents lists available at ScienceDirect

Nuclear Materials and Energy

journal homepage: www.elsevier.com/locate/nme

A study on the density shoulder formation in the SOL of H-mode plasmas

D. Carralero[a,*], J. Madsen[b], S.A. Artene[a,c], M. Bernert[a], G. Birkenmeier[a,c], T. Eich[a], G. Fuchert[d], F. Laggner[a], V. Naulin[b], P. Manz[c], N. Vianello[e,f], E. Wolfrum[a], the EUROfusion MST1 team[1], the ASDEX Upgrade Team[a]

[a] Max Planck Institute for Plasma Physics, Boltzmannstr. 2, 85748 Garching, Germany
[b] Aalto University, Espoo, Finland
[c] Physik-Department E28, Technische Universität München, Garching, Germany
[d] Max Planck Institute for Plasma Physics, Greifswald, Germany
[e] Consorzio RFX, Padova, Italy
[f] Ecole Polytechnique Fédérale de Lausanne, Swiss Plasma Center (SPC), Lausanne, Switzerland

ARTICLE INFO

Article history:
Received 15 July 2016
Revised 20 October 2016
Accepted 18 November 2016
Available online 23 December 2016

PSI-20 keywords:
ASDEX-Upgrade
Detachment
Edge plasma
Intermittent transport
H-mode

ABSTRACT

The term “shoulder formation” refers to an increase of the density decay length in the scrape-off layer (SOL) observed in many tokamaks during L-mode operation when a density threshold is reached. Recent experiments in ASDEX Upgrade (AUG) and JET have shown that the shoulder forms when the divertor collisionality in the divertor electrically disconnects filaments from the wall. This leads to a transition from the sheath limited to the inertial regime and to an enhancement of radial particle transport, in good agreement with analytical models. In the present work, the validity of such a mechanism is investigated in the more reactor-relevant H-mode regime. For this, a cold divertor H-mode scenario is developed in AUG using different levels of D puffing and N seeding, in which inter-ELM filaments and SOL density profiles are measured. The basic relation between filament size and divertor collisionality is still valid in H-mode plasmas, albeit an additional condition related to the gas fueling rate has been found for the formation of the shoulder.

© 2016 The Authors. Published by Elsevier Ltd.
This is an open access article under the CC BY-NC-ND license.
(http://creativecommons.org/licenses/by-nc-nd/4.0/)

1. Introduction

The next generation of magnetic confinement fusion devices will need to solve the problem of extreme heat and particle fluxes on Plasma-Facing Components (PFC), which will almost certainly stretch available materials to their technical limits on power loads and erosion levels [1]. In particular, the prediction of particle and heat fluxes onto the main vessel components will require the development of a working model for perpendicular transport in the far Scrape-off Layer (SOL), including the propagation of filamentary structures [2]. Recent work carried out in ASDEX Upgrade (AUG) [3] advanced in this direction by confirming experimentally the predictions of analytical models for filament propagation [4-6], which explained the broadening of L-mode SOL density profiles observed in many tokamaks (sometimes referred to as “density shoulder”) [7,8] in terms of a filament regime transition. It was shown how the parameter regulating shoulder formation is the effective divertor collisionality, Λ_{div} [5]. When this parameter, representing the product of characteristic parallel transport time and the ion-electron collision frequency in the divertor region, becomes $\Lambda_{div} > 1$, filaments electrically disconnect from the wall thus transitioning from the sheath limited [4] to the inertial regime [6]. This greatly enhances radial transport.

According to these findings, baseline scenarios for ITER and DEMO would feature fully developed density shoulders, as the estimated values of Λ_{div} will greatly exceed that threshold [9]. This could be of great practical importance, since it could substantially increase the particle flux arriving at the first wall, as well as contribute to spread particle and power fluxes on the divertor target. Both effects would have relevant consequences for the sputtering yield from the PFCs of both regions, thus changing the life times of several components. However, so far the regime transition model

* Corresponding author.
E-mail address: daniel.carralero@ipp.mpg.de (D. Carralero).
[1] See http://www.euro-fusionscipub.org/mst1

http://dx.doi.org/10.1016/j.nme.2016.11.016
2352-1791/© 2016 The Authors. Published by Elsevier Ltd. This is an open access article under the CC BY-NC-ND license. (http://creativecommons.org/licenses/by-nc-nd/4.0/)

Table 1
Main parameters of the discharges. The four scenarios A-D are grouped in four colors (respectively, blue/green/black/red), based on their D_{rate}, N_{rate} values.

Shot	Scenario	P_{ECH} (MW)	P_{NBI} (MW)	$D_{rate\ t=3.5\ s}$ (10^{21} s^{-1})	$N_{rate\ t=4.5\ s}$ (10^{21} s^{-1})	D_{rate} max (10^{21} s^{-1})	N_{rate} max (10^{21} s^{-1})	$T_{e,div}$ min (eV)
31974 (○)	A) Low N, Low D	1.3	-	1.3	2.8	1.3	3.4	1
31977 (□)		1.9	-	1.3	2.8	1.3	3.8	0
33055 (○)	B) High N, Low D	1.3	1.7	6	1.8	6	8	1.5
33057 (□)		1.3	1.7	8.2	1.8	8.2	8	3
33056 (○)	C) High D, no N	1.3	1.7	6.3	-	24.5	-	10
33058 (○)	D) High D, High N	1.3	1.7	6.3	2	15.4	8	5
33059 (□)		1.3	1.7	6.3	4	24	4	5
33475 (◊)		1.4	1.7	6.2	5	24.4	5	7.5
33478 (Δ)		1.4	2.4	7	9.2	24.4	9.2	1.5

has only been tested in L-mode plasmas, while next generation devices will operate in H-mode. Therefore, it is necessary to prove that shoulder formation does also happen in H-mode, and if so, that the same mechanism found in L-mode applies. Regarding the first question, several examples of an H-mode shoulder formation can be found in the literature [10,11], but no systematic study has been realized so far. Besides, this problem must be separated from ELM-related transport, which usually dominates the SOL of present day machines operating in H-mode, as ITER and especially DEMO will most likely feature substantially reduced levels of ELM activity [12]. In the present work, we present the results of a series of experiments carried out on AUG with the aim of inducing a shoulder formation during inter-ELM H-mode periods in order to validate the filament transition model by measuring the evolution of filaments and Λ_{div} during the process.

2. Experiments

In order to evaluate the filament transition model, the evolution of filament characteristics and SOL density profiles required to be measured while Λ_{div} was varied across the L-mode threshold ($\Lambda_{div} \in [0.1, 10]$) in an otherwise stationary H-mode plasma. Thus, a new scenario was developed using the same magnetic geometry (LSN edge optimized configuration) and plasma parameters ($B_T = -2.5$ T, $I_p = 800$ kA, $q_{95} = 4.85$) as in L-mode discharges used in the previous work [3]. Sufficient ECH and NBI power was added to access the H-mode, while keeping the total heating power low enough to allow midplane manipulator (MPM) measurements with a multipin probe head as the one used in previous L-mode experiments [3]. Main parameters of the considered discharges are presented in Table 1. Given the power limitation, this scenario is far from LFS divertor detachment hence nitrogen seeding was required to obtain a cold, collisional divertor. In order to disentangle the effects of nitrogen and deuterium fueling on the Λ_{div} values, different fueling rates for both gases (N_{rate} and D_{rate}) were used, roughly dividing the data set in four scenarios: A) low power discharges with low N_{rate} and D_{rate} values; B) discharges including both NBI and ECH heating, strong nitrogen seeding and a low D_{rate}; C) A discharge in which $\Lambda_{div} > 1$ is achieved only by means of a strong density fueling with no nitrogen; D) discharges with full power, and both high N_{rate} and D_{rate} values.

A typical discharge is presented in Fig. 1, where three phases can be distinguished: first, only 300 kW of ECRH heating power is used to establish a reference L-mode. Next, full NBI and ECRH power is injected and H-mode with type-I ELMs is accessed. Finally, the Λ_{div} scan is carried out by increasing N_{rate} and/or D_{rate}. This ends the type-I ELMs and replaces them with smaller, more frequent ones. Also, the divertor temperature is reduced, bringing the LFS divertor to different levels of detachment. During the whole discharge, divertor conditions and midplane density profiles are measured, respectively, by a set of divertor fixed Langmuir probes [13] and the lithium beam diagnostic [14]. Also, the evolution of the main plasma density is monitered using a line-integrated interferometer measurement covering the region outside the $\rho > 0.875$ flux surface [15]. Λ_{div} is calculated as explained in [3], using divertor target values of n_e and T_e and a 1/5 fraction of $\pi R q_{95}$ as the characteristic parallel length (where R is the major radius of AUG, and q_{95} is the safety factor near the separatrix). Additionally, the probe head in the MPM provides the perpendicular size and velocity of filaments by correlating ion saturation current measurements in poloidally and radially separated pins [15]. As can be seen in Fig. 1, the MPM is plunged multiple times during the discharge, covering each phase, and several values of Λ_{div}.

3. Analysis and results

3.1. ELM conditional averaging

In H-mode plasmas, ELMs introduce a new level of complexity in the present analysis: in L-mode, fluctuations do not substantially alter the background conditions of the SOL, and both divertor conditions and midplane density profiles can be measured separately. However, the ejection of ELMs in H-mode creates a major and intermittent perturbation across the whole SOL. Therefore, the ELM cycle has to be taken into account when defining the turbulent characteristics of transport. With this aim, the H-mode phase of each discharge is divided in 250 ms windows (which provide a sufficient number of events) and ELMs are detected using the thermoelectric current to the divertor, I_{div} [16]. This current is mainly caused by the temperature difference between the inner and outer divertor. Since the inner target is typically cold, I_{div} is a good measure of the temperature in the outer divertor and it is thus routinely used for the detection of ELMs in AUG. Then divertor Langmuir probes and lithium beam measurements are synchronized with I_{div} in order to obtain a conditionally averaged evolution of Λ_{div} and midplane n_e profiles as a function of $t-t_{E,max}$, where $t_{E,max}$ is the time of the maximum I_{div} value. Finally, for each window, pre-ELM ($t-t_{E,max} = -2$ ms) density and collisionality values are taken, as representative of the inter-ELM conditions [17]. The fraction of the ELM cycle corresponding to such inter-ELM state increases as the size of ELMs is reduced, going typically from around 20% for type-I ELMs to over 65% for the small ELMs found at the end of the discharges. This method is not applicable for MPM data, for which only the limited intervals in which

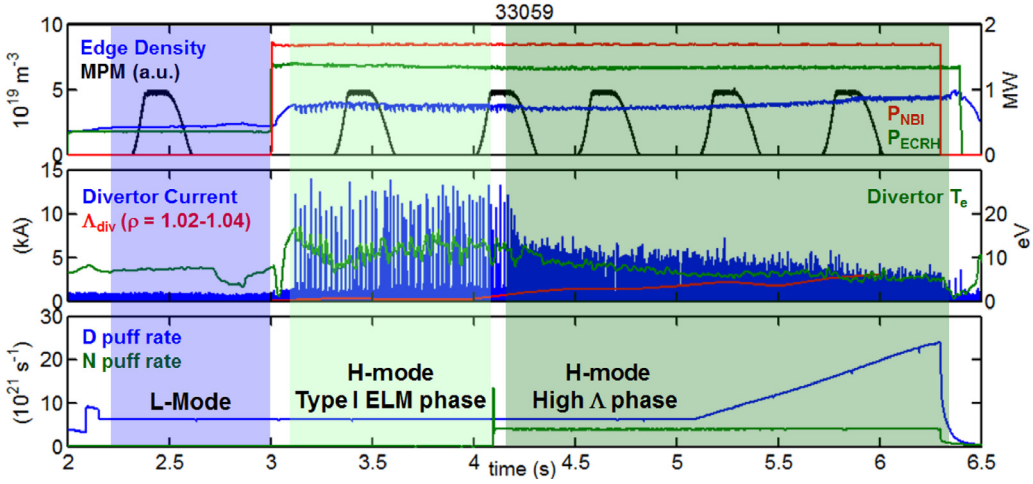

Fig. 1. The three phases on a typical discharge. Top) Edge line integrated density N_{edge} (blue) and heating power (P_{ECH} in green, P_{NBI} in red) are shown along with the radial position of the MPM (black). Middle) Divertor thermoelectric current (indicative of ELM activity), divertor T_e and Λ_{div} in the $\rho = 1.02–1.04$ area of the target in blue, red and green, respectively. Bottom) Deuterium fueling and N seeding rates D_{rate} (blue) and N_{rate} (green). (For interpretation of the references to color in this figure legend, the reader is referred to the web version of this article.)

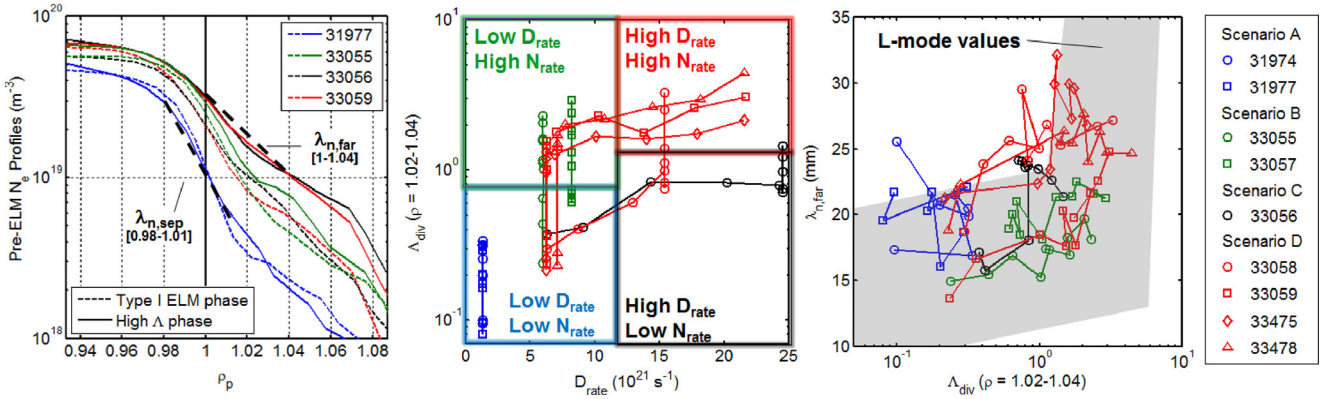

Fig. 2. Experimental results. a) Several inter-ELM Lithium beam density profiles during the two H-mode phases of the discharge. Separatrix and far SOL e-folding lengths $\lambda_{n,sep}$ and $\lambda_{n,far}$ are indicated. b) Parameter diagram, where the collisionality and D_{rate} of each discharge are displayed. c) Evolution of inter-ELM $\lambda_{n,far}$ with Λ_{div} for the whole set of discharges. The shaded area represents the range of L-mode values shown in [3]. The color code in all plots corresponds to the four scenarios A-D presented in Table 1. (For interpretation of the references to color in this figure legend, the reader is referred to the web version of this article.)

the manipulator is inserted are available. In this case, I_{div} is used to separate "inter-ELM" probe data from "close to an ELM" data (i.e., $3\ ms > t - t_{E,max} > -2\ ms$). Then, filament conditional analysis is performed on "inter-ELM data" using a 2.5σ threshold, as in previous work [15].

3.2. Shoulder formation

According to the model valid in L-mode, in those discharges in which the D_{rate} and/or N_{rate} are high enough to achieve $\Lambda_{div} > 1$, a shoulder formation should be observed by the end of the third phase (high collisionality H-mode). In Fig. 2a, some inter-ELM density profiles are presented at the beginning of the H-mode ($t = 3.75$ s, dashed lines) and at the end of the third phase ($t = 6$ s, solid lines). As can be seen, discharges #33056 and #33059 exhibit a clear flattening at the end of the discharge, while in the other two cases little or no flattening can be seen in the same interval. In order to quantify this effect, two e-folding lengths are defined on the profiles: First, $\lambda_{n,far}$, representing the gradient of the profile in the far SOL, is fitted in the radial range $\rho_p \in [1, 1.04]$. This parameter is equivalent to the λ_n used in previous works to detect the shoulder formation [3, 15]. Second, $\lambda_{n,sep}$, representing the evolution around the separatrix, is fitted in the range $\rho_p \in [0.98, 1.01]$. Also, Λ_{div} is calculated using the fixed divertor probes in the range $\rho_p \in [1.02, 1.04]$. In Fig. 2b, the evolution of Λ_{div} through the discharge is represented as a function of D_{rate} in the four scenarios described in Section 2. The same color code is used as in Table 1 (respectively, blue/green/black/red for scenarios A-D). As can be seen, independently of the levels of D_{rate} only scenarios with high N_{rate} clearly surpass the $\Lambda_{div} > 1$ threshold. Instead, the low N_{rate}, low D_{rate} scenario remains clearly under the threshold, and the one with no nitrogen surpasses slightly $\Lambda_{div} = 1$ by the end of the discharge. The differences between the four scenarios can be seen in Fig. 2c, where the relation between inter-ELM Λ_{div} and $\lambda_{n,far}$ is shown using the same color code over a shaded background representing the trend found in L-mode experiments. Considering the point cluster as a whole, a behavior similar to that of L-mode is found, with $\lambda_{n,far}$ rising when $\Lambda_{div} > 1$, even if the increase is not as sharp and the $\lambda_{n,far}$ values are not as high. However, when the four scenarios are considered individually, a clearer trend is found: discharges from scenario A display low levels of Λ_{div} and do not access the higher transport regime. The same is valid essentially for scenario C, albeit slightly higher Λ_{div} (and thus $\lambda_{n,far}$) values are achieved. Instead, all discharges from scenario D develop a clear shoulder, achieving a significant increase in $\lambda_{n,far}$ at higher values of Λ_{div}. Interestingly, discharges in scenario B, displaying similar Λ_{div} values as those in scenario D, fail to achieve high $\lambda_{n,far}$ values.

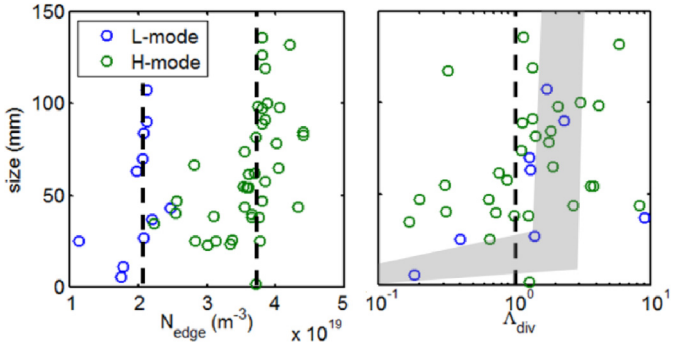

Fig. 3. Inter-ELM filament size. a) As a function of line integrated edge density. b) As a function of Λ_{div}. Shaded area corresponds to L-mode values from [3]. Color indicates L/H-mode. (For interpretation of the references to color in this figure legend, the reader is referred to the web version of this article.)

3.3. Filament characteristics

The main results from a conditional analysis of MPM data are shown in Fig. 3: the evolution of the filament size with the edge line-integrated density shows two thresholds above which the size increases sharply: the first one, observed in the L-mode phase, takes place around $N_{edge} = 2 \times 10^{19}\,m^{-3}$, and coincides with the L-mode shoulder formation detected previously for 300 kW operation [3]. The second, observed in H-mode, is observed around $N_{edge} = 3.75 \times 10^{19}\,m^{-3}$, and would correspond to an equivalent threshold for H-mode. Instead, when the same data points are represented as a function of Λ_{div} in Fig. 3b, the two thresholds merge around $\Lambda_{div} = 1$, in good agreement with the expectations from the filament model, and suggesting that the same disconnection mechanism applies in H-mode. Still, as with the shoulder formation, the transition is not as clear as the one found in L-mode. Besides that, some properties of the filaments change when going from L to H-mode: first, as can be seen in Fig. 3, pre-transition filaments tend to be larger in size in H-mode. Also, the relative amplitude of filaments (expressed as the ratio between the standard deviation and the mean values of ion saturation pins, σ/μ) is increased by 30% in H-mode (from $\sigma/\mu \sim 0.35–0.4$ to $\sigma/\mu \sim 0.45–0.55$). This effect is mostly due to the reduction in density in the SOL, and disappears when σ/N_{edge} is used instead. Finally, the detection frequency is reduced for $\Lambda_{div} < 1$, with typical values in the range of $f_d \in [2000,2500]\,s^{-1}$ and $f_d \in [1000,1500]\,s^{-1}$ for L and H-mode, respectively. A word of caution is in order here, as f_d is most likely not only affected by the SOL conditions but also by the filament generation frequency, which can be expected to change substantially with the formation of the H-mode pedestal.

3.4. Near SOL evolution

Besides the evolution of $\lambda_{n,far}$, the relation of the density gradient at the separatrix with the process of shoulder formation has been observed: As shown in Fig. 4, by comparing $\lambda_{n,far}$ and $\lambda_{n,sep}$ in the dataset, it could be concluded that they are uncorrelated, and thus $\lambda_{n,sep}$ is neither correlated with the Λ_{div} parameter responsible for shoulder formation. Instead, $\lambda_{n,sep}$ seems to be clearly correlated to D_{rate} in discharges with variable levels of gas fueling (no such relation is found between N_{rate} and $\lambda_{n,sep}$, though). Also, the $\lambda_{n,sep}$ value is proportional to the ELM frequency.

4. Discussion and conclusions

The first conclusion could be that a phenomenon analogous to the well documented L-mode shoulder formation can be found when a density threshold is surpassed under certain conditions in inter-ELM periods of H-mode plasmas: indeed, as seen in Fig. 5a, some of the discharges have a sharp increase in $\lambda_{n,far}$ for $N_{edge} > 3.7 \times 10^{-19}\,m^{-3}$. As well, the role of Λ_{div} as the parameter regulating the formation of the shoulder seems to be also generally valid in H-mode: as can be seen in Fig. 2c, only discharges with $\Lambda_{div} > 1$ (namely those in scenario D) display a clear shoulder. In these cases, the inter-ELM LFS divertor is in a partial detachment state equivalent to the one found in L-mode discharges for equivalent Λ_{div} values. However, this study reveals a more complex picture than in L-mode, as $\Lambda_{div} > 1$ seems to be necessary but not sufficient for the shoulder formation: shots in scenario B do not reach high values of $\lambda_{n,far}$ despite a high collisionality in the divertor. As the data in Fig. 2 reveal, this happens for discharges with low D_{rate}, indicating the existence of a second threshold for the shoulder, related to the deuterium puffing level. This is not related to the fueling of the main plasma: as can be seen in Fig. 5a, a high N_{edge} does not trigger the shoulder formation either, since Scenario B reaches the same range of edge densities as Scenario D. Therefore, the mechanism relating fueling and shoulder formation can probably be found in the SOL. One possible explanation for this would be that the shoulder formation requires a high recycling rate at the main wall on top of the increased convective transport [18]. This would be in good agreement with recent experiments which show how far-SOL ion temperatures drop after the shoulder formation [19,20], suggesting that a large fraction of the ions in it do not come from the confined plasma but from ionization of recycled neutrals. In such a case, a minimum level of neutral density in the far SOL could be required to start the process, thus requiring a minimum value of D_{rate}. The precise determination of this second threshold and the identification of the underlying physical mechanism will be the subject of forthcoming work.

A second conclusion would be that a similar regime transition seems to take place as in L-mode, since the filament size is substantially increased when high collisionality disconnects the SOL from the wall. Also, the relation between transition in the filament dynamics and shoulder formation seems to hold in H-mode, as they both share the same Λ_{div} and N_{edge} thresholds. A more direct comparison can be seen in Fig. 5b, where the sizes of filaments measured during some discharges from Fig. 2 are shown. A general correlation between filament size and $\lambda_{n,far}$ appears, suggesting a relation between increased filamentary transport and the flattening of the profiles. This correlation would also mean that large filaments only appear when a shoulder is formed. However, filament and density data are not both available in all cases (not all discharges had the MPM equipped with the right probe head, probe data is limited to the reciprocations, etc.), so given the limited amount of data and the large error bars in the filament size calculation, no conclusive statement can be made yet. The clarification of this subject will also be addressed in forthcoming works.

Finally, the density gradient length around the separatrix has been found to be largely independent of the collisionality at the divertor, but correlated to D_{rate} and proportional to the ejection frequency of ELMs. The evolution of $\lambda_{n,sep}$ with D_{rate} and N_{rate} is consistent with recent studies on the high-field side high density (HFHSD) region in AUG [21,22]. This region, which tends to flatten the density gradient at the separatrix, forms as D_{rate} is increased (which would correspond in Fig. 4a to the increase of $\lambda_{n,sep}$ when going from Scenario A to B and from B to C) and has been proven to be strongly reduced with nitrogen seeding (which would correspond in Fig. 4a to the reduction of $\lambda_{n,sep}$ from Scenario C to D).

Summarizing, the formation of a shoulder has been observed in inter-ELM H-mode plasmas. The general link between shoulder formation and filament transition also seems to remain valid. Collisionality remains the necessary condition for the shoulder formation, but deuterium fueling seems to play an additional role. These results allow the extension of the general shoulder

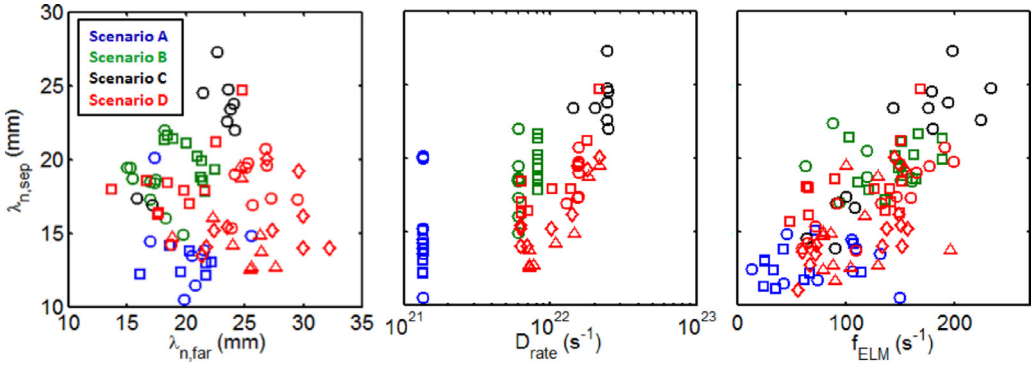

Fig. 4. Inter-ELM separatrix density e-folding length, $\lambda_{n,sep.}$ a) as a function of $\lambda_{n,far}$. b) as a function of puffing rate D_{rate}. c) As a function of ELM frequency. Color code as in Fig. 2. (For interpretation of the references to color in this figure legend, the reader is referred to the web version of this article.)

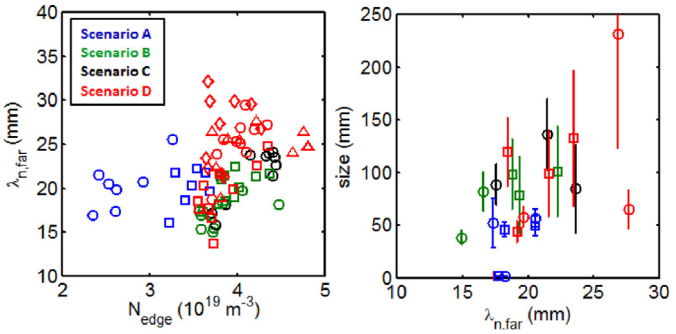

Fig. 5. a) Relation between filament size and $\lambda_{n,far}$. b) Scaling of $\lambda_{n,far}$ with edge line integrated density, N_{edge}. Same set of discharges and color code as in Fig. 2. (For interpretation of the references to color in this figure legend, the reader is referred to the web version of this article.)

formation mechanism validated in L-mode to H-mode plasmas with the introduction of a few new elements. Future work will address the interplay of filamentary transport and neutral penetration in the SOL in order to clarify the precise mechanism relating D_{rate} with $\lambda_{n,far}$. This is a necessary step on the way to a general scaling of the SOL width, capable of improving current predictions for ITER and DEMO operation.

Acknowledgments

This work has been carried out within the framework of the EUROfusion Consortium and has received funding from the Euratom research and training programme 2014–2018 under grant agreement No 633053. The views and opinions expressed herein do not necessarily reflect those of the European Commission.

References

[1] A. Loarte, M. Sugihara, M. Shimada, et al., 22nd IAEA Fusion Energy Conference, 2008.
[2] S.I. Krasheninnikov, Phys. Lett. A 238 (2001) 368–370.
[3] D. Carralero, P. Manz, L. Aho-Mantila, et al., Phys. Rev. Lett. 115 (2015) 215002.
[4] S.I. Krasheninnikov, D.A. D'Ippolito, J.R. Myra, J. Plasma Phys. 74 (2008) 679717.
[5] J.R. Myra, D.A. Russell, D.A. DÍppolito, Phys. Plasmas 13 (2006) 112502.
[6] O.E. Garcia, R.A. Pitts, J. Horacek, et al., J. Nucl. Mater. 363–365 (2007) 575–580.
[7] B. LaBombard, R.L. Boivin, M. Greenwald, et al., Phys. Plasmas 8 (2001) 2107.
[8] D.L. Rudakov, J.A. Boedo, R.A. Moyer, et al., Nucl. Fusion 45 (2005) 1589–1599.
[9] D. Carralero, H.W. Müller, M. Groth, et al., J. Nucl. Mater. 463 (2015) 123–127.
[10] H.W. Müller, M. Bernert, D. Carralero, et al., J. Nucl. Mater. 463 (0) (2015) 739–743.
[11] H.J. Sun, E. Wolfrum, T. Eich, et al., Plasma Phys. Control Fusion 57 (12) (2015) 125011.
[12] R.P. Wenninger, M. Bernert, T. Eich, et al., Nucl. Fusion 54 (2014) 114003.
[13] M. Weinlich, A. Carlson, Contrib. Plasma Phys. 36 (S) (1996) 53–60.
[14] M. Willensdorfer, G. Birkenmeier, R. Fischer, et al., Plasma Phys. Control Fusion 56 (2014) 025008.
[15] D. Carralero, G. Birkenmeier, H.W. Müller, et al., Nucl. Fusion 54 (2014) 123005.
[16] A. Kallenbach, R. Dux, J.C. Fuchs, et al., Plasma Phys. Control Fusion 52 (2010) 055002.
[17] A. Burckhart, E. Wolfrum, R. Fischer, et al., Plasma Phys. Control Fusion 52 (2010) 105010.
[18] B. Lipschultz, D. Whyte, B. LaBombard, Plasma Phys. Control Fusion 47 (2005) 1559–1578.
[19] D. Carralero, H.J. Sun, S.A. Artene, et al., 42th EPS Conference on Plasma Physics, Lisbon, Portugal, 2015.
[20] S.Y. Allan, S. Elmore, G. Fishpool, et al., Plasma Phys. Control Fusion 58 (2016) 045014.
[21] S. Potzel, M. Wischmeier, M. Bernert, J. Nucl. Mat. 463 (2015) 541–545.
[22] F. Reimold, M. Wischmeier, S. Potzel, et al., J. Nucl. Mat. Energy (2016).